Myosin Light-Chain Domain Rotates upon Muscle Activation but Not ATP Hydrolysis[†]

Ingrid Brust-Mascher, Leslie E. W. LaConte,[‡] Josh E. Baker, and David D. Thomas*

Department of Biochemistry, Molecular Biology, & Biophysics, University of Minnesota Medical School, Minneapolis, Minnesota 55455

Received March 16, 1999; Revised Manuscript Received July 1, 1999

ABSTRACT: We have studied the correlation between myosin structure, myosin biochemistry, and muscle force. Two distinct orientations of the myosin light-chain domain were previously resolved using electron paramagnetic resonance (EPR) spectroscopy of spin-labeled regulatory light chains in scallop muscle fibers. In the present study, we measured isometric force during EPR spectral acquisition, in order to define how these two light-chain domain orientations are coupled to force and the myosin ATPase cycle. When muscle fibers are partially activated with increasing amounts of calcium, the distribution between the two light-chain domain orientations shifts toward the one associated with strong actin binding. This shift in distribution is linearly related to the increase in force, suggesting that rotation of the light-chain domain is coupled to strong actin binding. However, when nucleotide analogues are used to trap myosin in the pre- and posthydrolysis states of its ATPase cycle in relaxed muscle, there is no change in the distribution between light-chain domain orientations, showing that the rotation of the light-chain domain is not directly coupled to the ATP hydrolysis step. Instead, it is likely that in relaxed muscle the myosin thick filament stabilizes two light-chain domain orientations that are independent of the nucleotide analogue bound at the active site. We conclude that a large and distinct rotation of the light-chain domain of myosin is responsible for force generation and is coupled to strong actin binding but is not coupled to a specific step in the myosin ATPase reaction.

The fundamental conformational change responsible for force generation and sarcomere shortening in contracting muscle has been proposed to be a large rotation of the light-chain (LC)[1] domain of myosin (*1, 2*). This rotation was recently observed using EPR spectroscopy, by showing that a spin label on the regulatory light chain (RLC) rotates through an axial angle of at least 36° upon force generation (*3*). The simplest model of lever-arm action is that the LC domain rests in one orientation and rotates to a second orientation upon strong actin binding to produce force. However, the unique orientational resolution of EPR led to the surprising discovery that, in relaxed scallop muscle, the spin-labeled LC domain is equally distributed between two orientations (M1 and M2), and contraction coincides with a fraction of myosin heads undergoing at least a 36° rotation of the LC domain from M1 to M2 (*3*), the orientation associated with strong actin binding.

The findings that two orientations of the LC domain exist in relaxed muscle and that the strong-binding LC domain structure is present in both relaxed and contracting muscle

were initially perplexing. However, there is ample evidence for these two distinct structures in relaxed muscle. Early X-ray diffraction data (*4*) and recent helical reconstructions of electron micrographs (*5*) suggest that, under relaxation conditions, the two heads of a scallop myosin dimer adopt a "splayed" configuration in which they are axially separated from one another. It has also been shown that myosin heads can be cross-linked intermolecularly, consistent with a splayed configuration (*6*). The two distinct LC domain structures we observe in relaxed muscle are also consistent with models derived to explain myosin kinetics (*7*) and muscle fiber kinetics (*8*), since these models require cooperativity between the two heads of the myosin dimer.

The X-ray diffraction and electron microscopy experiments mentioned above showed that relaxed muscle is well-ordered and that activation of muscle then leads to disorder within the fiber (*9*). These data would imply that force generation coincides with an increase in disorder. This is in sharp contrast to models of muscle contraction that conclude that a disorder-to-order transition within the myosin head is responsible for generating force (*10−12*). This apparent conflict has been difficult to resolve.

In the present study, we examine the correlation between myosin structure, force, and the ATP hydrolysis step, to discover what determines the distribution between the two LC domain structures. EPR spectroscopy is crucial to this study because it provides spectral resolution of orientational populations of the LC domain when a labeled muscle fiber is oriented in the magnetic field (*13*). Here we report simultaneous detection of isometric force and EPR spectra
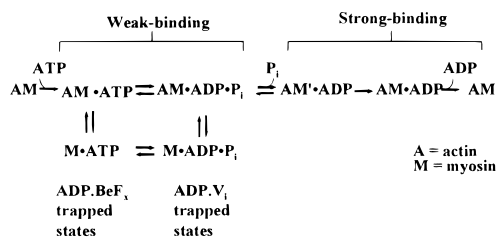
* To whom correspondence should be addressed. Phone: (612) 625-0957. Fax: (612) 624-0632. E-mail: ddt@ddt.biochem.umn.edu.

[‡] I.B.M. and L.E.W.L. contributed equally to this work.

[1] Abbreviations: EPR, electron paramagnetic resonance; FDNASL, 3-(5-fluoro-2,4-dinitroanilino)-2,2,5,5-tetramethyl-1-pyrrolidinyloxy; LC, light chain; RLC, regulatory light chain.

Scheme 1

in spin-labeled scallop muscle fiber bundles. This is a significant advance in experimental technique, since both mechanical and structural states of the same sample are studied simultaneously. Our experimental design thus allows us to correlate muscle force with the distribution between M1 and M2 LC domain orientations. To understand the coupling between the distribution of LC domain orientations and muscle force, we partially activate muscle by increasing the levels of calcium during spectral acquisition and force measurement. This experiment allows direct correlation of myosin structure and muscle force.

EPR spectroscopy of the spin-labeled LC domain in muscle fibers also allows us to correlate myosin structural changes with the myosin-catalyzed ATP hydrolysis reaction. Scheme 1 shows the standard model coupling the myosin ATPase cycle to the interaction of actin and myosin. In this scheme, the prehydrolysis and posthydrolysis (M·T and M·D·P_i) biochemical states are weak-binding states, meaning that myosin binds very weakly to actin (*14*) and produces no force. In relaxed muscle, all weak-binding biochemical states are present, and both M1 and M2 myosin structures are equally populated (*3*). Nucleotide analogues are commonly used to trap different intermediates of the ATPase cycle. Beryllium fluoride (BeF$_x$) was recently identified as a phosphate analogue in myosin (*15*) and, when in a complex with ADP, closely mimics the structure of unhydrolyzed ATP (*16*−*18*). Vanadate (V$_i$), another phosphate analogue of myosin, has been proposed to trap myosin heads in the posthydrolysis state in the presence of ADP (*19*). These analogues can be employed to study the coupling of the ATP hydrolysis step to the myosin structures in relaxed muscle.

The resolution of M1 and M2 in muscle has allowed us to directly observe the coupling between myosin biochemistry, myosin structural changes, and muscle force by monitoring both the orientation of the LC domain and isometric force. We have studied partially activated muscle fibers and muscle fibers trapped in the pre- and posthydrolysis states. The results in this paper suggest that while muscle force is directly coupled to the rotation of the LC domain, the LC domain rotation is not directly coupled to the ATP hydrolysis step.

MATERIALS AND METHODS

RLC Purification and Labeling. RLCs were purified from chicken gizzard myosin (*20*) and spin labeled with 3-(5-fluoro-2,4-dinitroanilino)-2,2,5,5-tetramethyl-1-pyrrolidinyloxy (FDNASL) by incubating 40 μM RLC with 100 μM FDNASL (pH 7, 4 °C) for 20 h. The spin/protein ratio was 0.9 ± 0.1, indicating complete and specific reaction with the single thiol on Cys 108.

Scallop Fiber Preparation and RLC Exchange. Fiber bundles were prepared from scallop (*Placopecten magel-*

lanicus) adductor muscle (*22*) without Triton treatment. Bundles of 1−2 mm were dissected and put in glass capillary tubes with an inner diameter of 1.0 mm and an outer diameter of 1.6 mm, tied on both ends with surgical silk thread to hold them isometrically. Some fibers were used immediately after dissection. Others were stored at −20 °C in 50% glycerol/50% buffer A (40 mM NaCl, 0.1 mM NaN$_3$, and 10 mM Mops, pH 7) with 2 mM MgCl$_2$ for later use. Native RLC was removed by perfusing buffer A with 15 mM EDTA over fibers at 10 °C for 30 min for partial extraction of one RLC per two-headed myosin dimer [[RLC]/[ELC] = 0.44 ± 0.04 (*n* = 14)]. Extracted fibers were incubated in buffer A plus 2 mM MgCl$_2$ and 2 mg/mL spin-labeled RLC for 2 h on ice, then perfused with buffer A plus 2 mM MgCl$_2$ for 15 min. To improve signal during EPR data acquisition, fibers were removed from capillaries, tied into bundles of two, and rethreaded through the capillaries.

Scallop muscle fibers, which have myosin-based calcium regulation, can be activated by partial removal of the RLC (constitutive activation). Readdition of both native RLC and RLC from chicken gizzard restores Ca^{2+} regulation (*21*). This allows a quantitative measure of functional RLC binding. Fully exchanged fibers are Ca^{2+} regulated. However, due to the nonlinear relationship between force and RLC content in scallop muscle (*22*), these fibers often produced a small contraction upon addition of ATP. Partially exchanged fibers reproducibly relaxed from rigor force upon addition of ATP and contracted with ATP and Ca^{2+} and were therefore used for these experiments. The two spectral components derived from EPR spectra are the same for partially and fully exchanged fibers. The distributions between these components are slightly different than previously reported for fully exchanged fibers (*3*) (see Results).

Force Measurements. For most fibers, isometric force was measured simultaneously during EPR spectrum acquisition (*23*). A small chamber containing a SensoNor Ackers 801 strain gauge (Aksjelskapet, Norway) was mounted onto the side plate of a Bruker TM$_{110}$ cavity modified to hold a glass capillary tube with inner and outer diameters of 1.0 and 1.6 mm, respectively, parallel to the magnetic field (*13*). The thread attached to one end of the fiber bundle was threaded into this tensiometer chamber and attached to the strain gauge using Devcon Duco Cement. The thread on the other end of the bundle was secured by placing Tygon tubing over the end of the capillary tube. The chamber was then closed with a seal containing a small hole through which solution was continuously flowed over the fibers using a LKB Microperpex peristaltic pump (Bromma, Sweden) at a rate of 0.2 mL/min.

Measurement of isometric force during EPR acquisition allowed us to correlate the distribution observed spectroscopically with the force generated by the fiber. All fibers were initially perfused with rigor buffer. Changing the solution to relaxation buffer caused either no change in force or a decrease in force, indicating the presence of rigor force. Fibers that contracted in relaxation buffer were discarded. After relaxation, the buffer was changed either to a solution containing a nucleotide analogue or to contraction buffer. Differences in force between relaxation and subsequent addition of nucleotide analogues were measured by calculating the average isometric force before and after buffer change. Upon activation, the average maximum tension

generated by an isometrically contracting scallop muscle fiber was approximately 15 kN/m^2.

EPR Acquisition and Analysis. High-resolution detection of the LC domain probe orientation was obtained from EPR spectra of fiber bundles during continuous buffer perfusion and force acquisition. X-band EPR spectra of muscle fibers were acquired as previously described (*24*) in a Bruker ESP 300 spectrometer (Bruker Instruments, Billerica, MA). All EPR spectra were fit well by a sum of two spectral components corresponding to the M1 and M2 LC domain orientations (*3*). Each spectral component has a well-defined low-field peak. As the percentage of a component decreases, so does the intensity of the corresponding peak. Therefore, the ratio of the two low-field peaks provides a sensitive measure of spectral component composition. Spectral simulations were used to develop a curve relating low-field peak-height ratio to the mole fraction of the M2 component (X2). Each experimental spectrum was analyzed by measuring the ratio of these two peaks to obtain the mole fraction of M2 (X2).

Reagents and Solutions. Rigor buffer contained 20 mM Mops, 5 mM MgCl$_2$, 1 mM EGTA, and 0.1 mM NaN$_3$. Relaxation and contraction buffers contained, in addition, 5 mM ATP, 20 mM creatine phosphate, and 0.25 mg mL^{-1} creatine phosphokinase; the contraction buffer had a pCa of 4.0. For calcium titration experiments, pCa values used were approximately 6.0, 5.8, 5.5, 5.3, and 5.0. For V$_i$ buffers, 1 mM V$_i$ (from a stock of 50 mM V$_i$, pH 10) was added to relaxation buffer (without creatine phosphate and creatine phosphokinase) containing 20 mM Epps instead of Mops to maintain a pH of 8.0, since at pH 8, the predominant V$_i$ species is orthovanadate (*25*). BeF$_x$ solution was made by adding 3 mM BeCl$_2$ and 30 mM NaF to relaxation solution without creatine phosphate and creatine phosphokinase. The ionic strength of all buffers was adjusted to 200 mM with potassium propionate. Creatine phosphokinase was supplied by Boehringer-Mannheim. All other reagents were supplied by Sigma.

RESULTS

Distribution of M1 and M2 under Physiological Conditions. Scallop muscle fiber bundles were spin-labeled on the LC domain of myosin by replacing the RLC with spin-labeled chicken gizzard RLC, resulting in spin-labeled muscle fibers with normal Ca^{2+} sensitivity of force and ATPase activity (*3*). The EPR spectrum (V) of these fibers oriented parallel to the magnetic field consists of two spectral components (V1 and V2), which correspond to two distinct orientations of the spin label on the LC domain of myosin: $V = (1 - X2)V1 + X2 \times V2$. The two LC domain structures that correspond to the two orientations of the spin label are referred to as M1 and M2 and are present in mole fractions $(1 - X2)$ and X2, respectively. The distribution between these two structures, defined by X2, depends on the physiological state of the muscle fiber, as previously described (*3*). Figure 1 shows EPR spectra in the physiological states of relaxation, contraction, and rigor. In relaxation, the fraction of LC domains in the M2 orientation (X2) is 0.53 ± 0.01 (*n* = 20). In contraction, X2 is 0.65 ± 0.01 (*n* = 17). In rigor, X2 is 0.80 ± 0.02 (*n* = 20). In the present study, we will explore changes in X2 upon perturbation of physiological states by partially activating fibers or by trapping myosin biochemical states with nucleotide analogues.
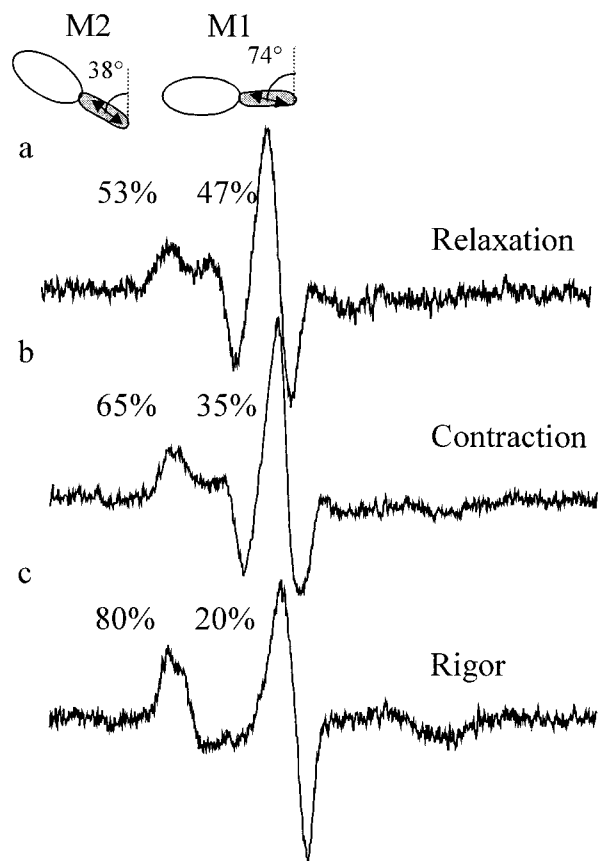

FIGURE 1: EPR spectra of scallop muscle fiber bundles partially exchanged with FDNASL-cgRLC in the physiological states of relaxation (a), contraction (b), and rigor (c). Each spectrum consists of two components that correspond to two orientations of the spin label on the LC domain as shown on top. The contribution from each component is shown above each spectrum.

Calcium Titration of Force and M2 Population. To determine the relationship between activated myosin heads, LC domain orientation, and force generation, we added increasing concentrations of Ca^{2+} to scallop fiber bundles. With increasing Ca^{2+} concentrations, myosin heads are recruited to bind strongly to actin (*26*). Figure 2 shows that force in the fiber bundles increased with increasing Ca^{2+} concentrations (a) and that the distribution shifted from M1 to M2 (b). Force increases linearly with increasing X2 (Figure 2c), which is the mole fraction of myosin heads in the strong-binding (force-bearing) orientation (*3*).

Trapping of Pre- and Posthydrolysis States. The weak-binding states present in relaxation are a mixture of prehydrolysis and posthydrolysis states. The EPR spectrum in relaxation (Figure 1) is composed of 53% of M2 (X2 = 0.53), indicating that the LC domains are nearly equally distributed between the M1 and M2 orientations. We used ADP and phosphate analogues to trap either prehydrolysis or posthydrolysis weak-binding biochemical states, and thus determine whether the M1/M2 distribution depends on the ATP hydrolysis step.

Beryllium fluoride, BeF$_x$, is a P$_i$ analogue that binds to myosin as MgADP·BeF$_x$ and mimics the prehydrolysis (M·ATP) state (*16*–*18*). Fibers were perfused with rigor buffer, followed by relaxation buffer. The perfusion buffer was next changed to one containing BeF$_x$ (3 mM), either in the presence of MgATP or MgADP. These buffers had no effect on the resting force (after addition of MgADP·BeF$_x$, force
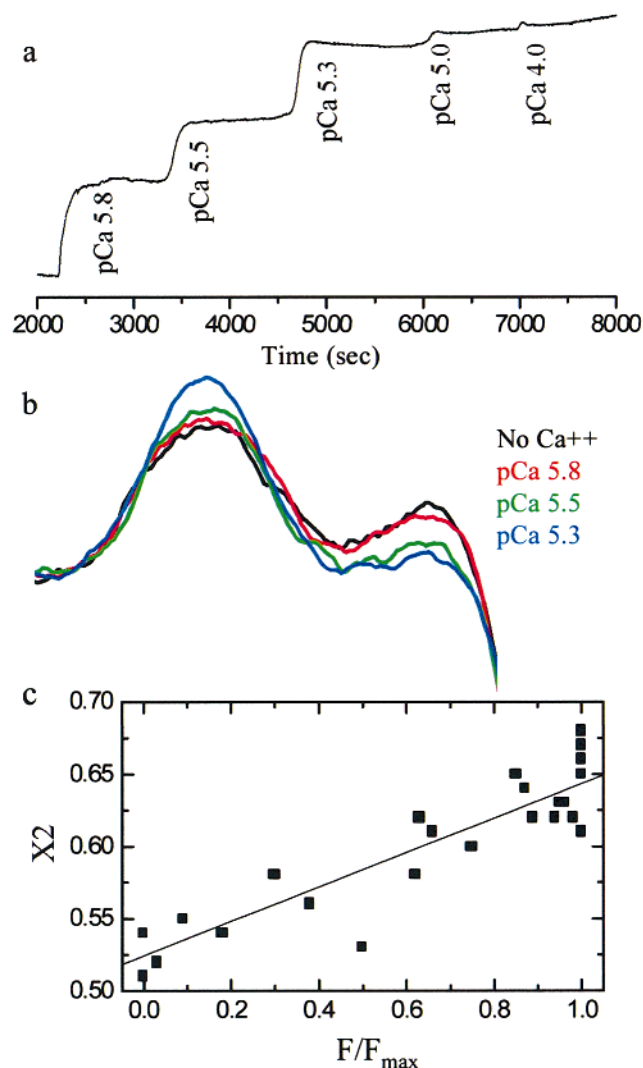
FIGURE 2: Effect of increasing calcium concentration on force and LC orientational distribution. (a) Force trace and (b) EPR spectra for one fiber. As force increases, the EPR spectrum shifts from that of relaxation toward that of contraction. Only the low-field peaks of the EPR spectra corresponding to M1 and M2 are shown. (c) X2 is a linear function of the muscle force. As force increases, more heads have the M2 conformation.
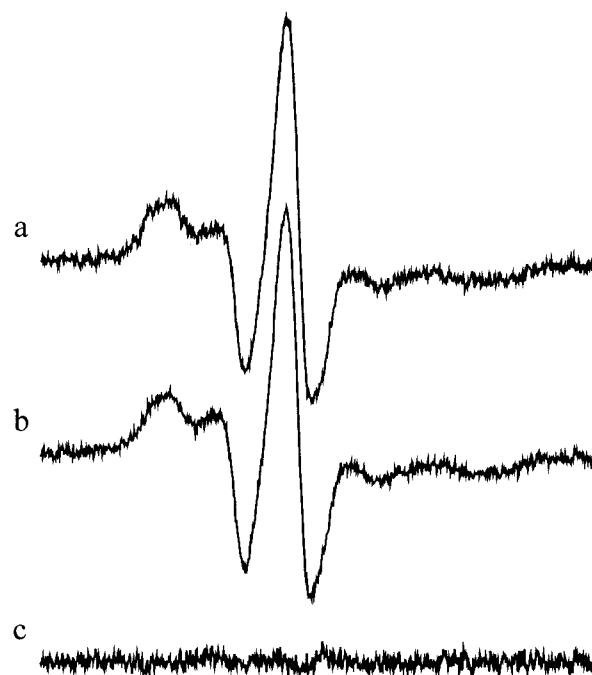

FIGURE 3: Addition of BeF_x to relaxed fibers. Spectra for a fiber in relaxation solution without (a) and with BeF_x (b) show that trapping the prehydrolysis state with $Mg \cdot ADP \cdot BeF_x$ does not change the distribution. (c) Difference spectrum.
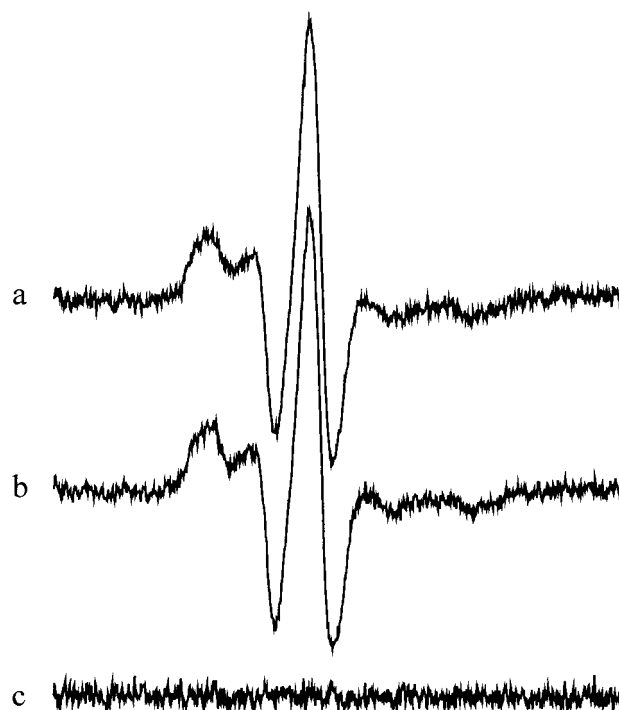

FIGURE 4: Addition of V_i to relaxed fibers. Spectra for a fiber in relaxation solution without (a) and with V_i (b) show that trapping the posthydrolysis state with $Mg \cdot ADP \cdot V_i$ does not change the distribution. (c) Difference spectrum.

changed by less than 1% of the average maximum active force) or the EPR spectrum (Figure 3) (the mole fraction X2 changed by 0.0 ± 0.0032). When fibers were activated, active isometric force was depressed in the presence of 3 mM $MgADP \cdot BeF_x$, indicating that the analogue does bind to the active site (data not shown).

Vanadate, V_i, is a P_i analogue that binds to myosin as $MgADP \cdot V_i$ and mimics the posthydrolysis $M \cdot ADP \cdot P_i$ state (*19*). Again fibers started out in rigor solution, were switched into relaxation solution, and finally perfused with a solution containing 1 mM V_i. Addition of V_i in the presence of MgATP or MgADP to relaxed fibers also had no effect on the resting force (fiber force changed by less than 1% of the average maximum force after addition of $MgADP \cdot V_i$) or on the EPR spectrum (Figure 4) (the mole fraction X2 changed by 0.0033 ± 0.0033). When fibers were activated, active isometric force was depressed by 76% after the addition of 1 mM $MgADP \cdot V_i$, indicating that the analogue does bind to the active site (*27*). The results from the V_i and BeF_x experiments indicate that the two structures, M1 and M2,

and the distribution between these are independent of the ATP hydrolysis step. Instead they are both present in a nearly equal distribution before and after ATP hydrolysis.

DISCUSSION

M1-to-M2 Rotation Is Directly Coupled to Force Generation. The simultaneous measurement of force and myosin

structure in muscle fibers allows us to explore the relationship between myosin LC domain orientation and muscle force. To correlate muscle force with the LC domain structural distribution, we added increasing amounts of submaximal Ca^{2+} to increase the number of active myosin heads (*26*). Calcium activates muscle fibers, recruiting myosin heads to bind strongly to actin and generate force. We observe that, with increasing Ca^{2+}, the fraction of heads in the M2 orientation, X2, increases linearly with force, indicating that the change in the fraction of strong-binding (force-bearing) myosin heads is directly related to the change in X2. Thus, force generation upon muscle activation is directly coupled to a rotation of a fraction of myosin heads from M1 to M2.

LC Domain Orientation in Relaxed Muscle Is Not Coupled to the ATP Hydrolysis Step. By using P_i analogues to trap myosin heads in the weak-binding biochemical states, M·ATP and M·ADP·P_i, we have shown that the LC domain of myosin is equally distributed between M1 and M2, regardless of which biochemical state is trapped. Therefore, the ATP hydrolysis step has no effect on the orientation of the LC domain with respect to the muscle filament axis in intact muscle fibers.

LC Domain Distribution in Relaxed Muscle Is Stabilized by Thick Filament. Since the ATP hydrolysis step does not affect the distribution between M1 and M2 in relaxed muscle, the most plausible explanation for this distribution is that the coiled coil of the myosin thick filament stabilizes the two heads of the myosin dimer. This supports the model of axially splayed heads first suggested by X-ray diffraction (*28*) and further supported by electron microscopy (EM) (*29*) data of myosin filaments from striated scallop muscle. Our results indicate that in scallop muscle, the myosin heads are axially separated by at least 36° (*3*). The splayed head arrangement does not appear to be unique to scallop muscle, according to reconstructions of negatively stained thick filaments [arthropod muscle (*30, 31*) and vertebrate striated muscle (*32*)], cross-linking studies [*Limulus* muscle (*6*) and vertebrate striated muscle filaments (*33*)], and EPR studies [vertebrate striated muscle (*3*)]. X-ray diffraction data obtained by Wray (personal communication) shows that, in relaxed scallop muscle, myosin heads are well ordered around the thick filament. This order is independent of temperature, suggesting that the structure of myosin heads in weak-binding states is determined by the filament lattice and not by temperature-sensitive biochemical states. Thus the present study confirms previous evidence for the splayed myosin head structure in relaxed muscle and shows how this structure changes upon muscle activation to generate force.

The presence of two LC domain orientations in relaxed muscle raises the long-asked question of the importance of the myosin dimer as the functional unit in muscle contraction (*34*). Single myosin heads are indeed capable of moving actin (*35*), but the importance of the second head is becoming increasingly clear. Recent in vitro motility assays on a recombinant *Dictyostelium* myosin II show that both sliding velocity and actin-activated ATPase activity decrease by at least half when single-headed myosin is used (*36*). Closer examination of myosin kinetics also support the conclusion of cooperativity between the two heads of the myosin dimer, both in scallop (*37*), as well as in vertebrate muscle (*38*).

Relationship to X-ray Crystal Structures of Myosin. The swinging lever arm hypothesis (*1*) has driven experimentalists to seek evidence for two distinct orientations of the LC domain with respect to the catalytic domain and to correlate the rotation between these orientations with a distinct biochemical step. To this end, nucleotide analogues have been used to crystallize myosin subfragment-1 (S1) intermediates in the myosin ATPase cycle. These crystal structures provide important, detailed information about the internal myosin head structure, including the angle between the catalytic and LC domains (*16, 39−45*). However, they do not provide information about how myosin heads are oriented with respect to the fiber axis in intact muscle. The relationship between myosin domain orientation and biochemical state must be understood in the context of the filament lattice of muscle. Therefore, in the present study, we have monitored the angle of the LC domain with respect to the actin filament in intact muscle fibers in the presence of different nucleotide analogues. The combination of these data and that obtained with other structural techniques yields a more complete description of how the angle between the catalytic domain and LC domain changes throughout the ATPase cycle in muscle.

EPR studies can provide information about both the orientation with respect to the muscle fiber axis and the dynamics of the internal myosin head structure. By spin labeling the LC domain, we have shown that, in weak-binding states, a bimodal LC domain orientation is present, probably stabilized by the myosin thick filament. Since the present study involves probes on the LC domain, the results do not directly reveal the angle between the catalytic and LC domains. However, previous EPR studies of both scallop myosin (*46*) and rabbit muscle fibers (*47−51*) with spin labels on the catalytic domain have consistently indicated that the catalytic domain is orientationally disordered with respect to actin in weak-binding states. This segmental flexibility has also been demonstrated with other probes placed on the LC domain (*52, 53*). We conclude that in weak-binding states there is significant segmental flexibility between the catalytic and LC domain (*10*).

Dynamic internal myosin flexibility has also been shown by other structural techniques. Significant flexibility within the myosin head (*54−56*) in weak-binding states is seen in electron micrographs of negatively stained myosin (*57*), which show that the conformation of S1 originally crystallized (*44*) is only rarely populated in solution. These data also show that the isolated myosin head has flexibility about the hinge between the catalytic and LC domains, even in the absence of nucleotide. The recently published crystal structure of the scallop myosin head, which includes the LC domain (*43*), also supports this conclusion. In this structure, the SH1 helix is unwound, resulting in significant flexibility in the converter region of the myosin head, which would allow the LC domain to adopt a number of different angles with respect to the catalytic domain. Thus, the myosin head is flexible, allowing the catalytic domain to rotate about a "hinge" relative to the LC domain. However, our results show that the ATP hydrolysis step does not cause an overall rotation of the LC domain with respect to the muscle fiber axis, as suggested previously (*45, 58*).

A number of different crystal structures of the myosin head have been determined, some of which suggest large changes in the angle between the catalytic domain and the LC domain, but no consistent pattern has emerged for how these
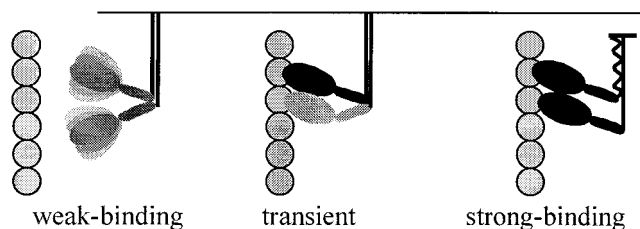
FIGURE 5: Structural model for muscle contraction. In weak-binding states, the thick filament stabilizes the LC domain of myosin. This leads to an equal distribution between the M1 and M2 LC domain orientations. The catalytic domain is disordered (*10*, *47−51*). Upon activation, one head of the dimer binds actin without an LC domain rotation. The second head forms a transient complex with the LC domain in the M1 orientation. The myosin head structure in this transient complex likely has a variable geometry (*12*) with respect to the angle between the catalytic and LC domain. Strong actin binding induces a rotation from the M1 to the M2 LC domain orientation.

structures correlate with the bound nucleotide (*42−44*). All crystal structures were obtained for the isolated S1 molecule, which is not stabilized by the muscle fiber lattice; any stabilization of a specific orientation between the two domains is enhanced by crystal-packing contacts. Crystallization tends to trap a single static structure, depending on buffer conditions and crystal contacts (*59*). The nucleotide present in the active site does not always determine which structure is trapped (*45*). This is not surprising since the fiber lattice plays an important role in the stabilization of myosin in vivo. The thick filament stabilizes the LC domain in weak-binding states, as shown here, and actin stabilizes the catalytic and LC domains, as shown here and in other studies.

Structural Model for Muscle Contraction. Because the thick filament stabilizes the splayed heads of the myosin dimer, relaxed muscle is well-ordered when examined by X-ray diffraction and EM. Upon activation, the muscle appears to become extremely disordered (*9*). These results have challenged researchers because it is difficult to develop a model of muscle contraction that includes an order-to-disorder transition. On the contrary, when the catalytic domain is probed, force development coincides with a disorder-to-order structural transition (*10−12*). Results from this paper and previous work on this system (*3*) help resolve this problem.

Figure 5 shows how the structurally ordered, relaxed myosin dimer can be activated to generate force in a muscle fiber. In weak-binding states, the LC domain of myosin is ordered in the splayed head configuration, as described above. The catalytic domain (*10*, *46−50*) is disordered on the microsecond time scale and samples different orientations about the flexible hinge separating the two domains (*55−57*). Upon strong actin binding, myosin's catalytic domain undergoes a disorder-to-order transition (*10−12*). One head of the dimer binds actin without a rotation of the LC domain, but the second head of the dimer forms a transient complex with the LC domain in the M1 orientation. According to recent studies by stopped-flow fluorescence and electron microscopy, this transient complex has a variety of different conformations (*12*). Actin binding induces a rotation of the LC domain, so that in strong-binding states, the myosin dimer is an M2−M2 complex. These transitions of myosin's internal structure to the strong-binding structure cause filament sliding and force generation.

CONCLUSIONS

We have studied the distribution of myosin structural states corresponding to two LC domain orientations, M1 and M2, and simultaneously measured isometric force. Calcium titration showed that some heads rotate from M1 to M2 during force generation and that the number of strong-binding heads in the M2 state is proportional to the generated force until maximal activation is reached. The use of nucleotide analogues to trap weak-binding intermediate states revealed that the distribution between M1 and M2 states is not coupled to the hydrolysis step; rather, all weak-binding states have a nearly equal distribution between the two structural states, probably determined by the interaction of the myosin dimer with the thick filament lattice. Filament sliding and force generation result from transitions between myosin's weak-binding structure, stabilized by the thick filament, and myosin's strong-binding structure, stabilized by actin.

REFERENCES

1. Rayment, I., Holden, H. M., Whittaker, M., Yohn, C. B., Lorenz, M., Holmes, K. C., and Milligan, R. A. (1993) *Science 261*, 58−65.
2. Uyeda, T. Q., Abramson, P. D., and Spudich, J. A. (1996) *Proc. Natl. Acad. Sci. U.S.A. 93*, 4459−4464.
3. Baker, J. E., Brust-Mascher, I., Ramachandran, S., LaConte, L. E. W., and Thomas, D. D. (1998) *Proc. Natl. Acad. Sci. U.S.A. 95*, 2944−2949.
4. Wray, J. S., Vibert, P. J., and Cohen, C. (1975) *Nature 257*, 561−564.
5. Vibert, P. (1992) *J. Mol. Biol. 223*, 661−671.
6. Levine, R. J. C., Chantler, P. D., and Kensler, R. W. (1988) *J. Cell Biol. 107*, 1739−1747.
7. Geeves, M. A., Goody, R. S., and Gutfreund, H. (1984) *J. Mus. Res. Cell Motil. 5*, 351−361.
8. Huxley, A. F., and Tideswell, S. (1997) *J. Muscle Res. Cell Motil. 18*, 111−4.
9. Vibert, P., and Craig, R. (1985) *J. Cell Biol. 101*, 830−837.
10. Thomas, D. D., Ramachandran, S., Roopnarine, O., Hayden, D. W., and Ostap, E. M. (1995) *Biophys. J. 68*, 135s−141s.
11. Bershitsky, S. Y., Tsaturyan, A. K., Bershitskaya, O. N., Mashanov, G. I., Brown, P., Burns, R., and Ferenczi, M. A. (1997) *Nature 388*, 186−90.
12. Walker, M., Zhang, X., Jiang, W., Trinick, J., and White, H. (1999) *Proc. Natl. Acad. Sci. U.S.A. 96*, 465−470.
13. Thomas, D. D., and Cooke, R. (1980) *Biophys. J. 32*, 891−906.
14. Eisenberg, E., and Hill, T. L. (1985) *Science 227*, 999−1006.
15. Phan, B. C., and Reisler, E. (1992) *Biochemistry 31*, 4787−4793.
16. Fisher, A. J., Smith, C. A., Thoden, J. B., Smith, R., Sutoh, K., Holden, H. M., and Rayment, I.. (1995) *Biochemistry 34*, 8960−8972.
17. Phan, B. C., Cheung, P., Stafford, W. F., and Reisler, E. (1996) *Biophys. Chem. 59*, 341−349.
18. Ponomarev, M. A., Timofeev, V. P., and Levitsky, D. I. (1995) *FEBS Lett. 371*, 261−263.
19. Goodno, C. C., and Taylor, E. W. (1982) *Proc. Natl. Acad. Sci. U.S.A. 79*, 21−25.
20. Persechini, A., and Hartshorne, D. J. (1983) *Biochemistry 22*, 470−476.
21. Simmons, R. M., and Szent-Györgyi, A. G. (1985) *J. Physiol. 358*, 47−64.

22. Simmons, R. M., and Szent-Györgyi, A. G (1980) *Natur*e *286*, 624−626.

23. Baker, J. E., Meyer, N. J., and Thomas, D. D. (1996) *Biophys. J. 70*, A266.

24. Roopnarine, O., and Thomas, D. D. (1995) *Biophys. J. 68*, 1461−1471.

25. Wells, C., and Bagshaw, C. R. (1984) *J. Mus. Res. Cell Motil. 5*, 97−112.

26. Kendrick-Jones, J., Lehman, W., and Szent-Györgyi, A. G. (1970) *J. Mol. Biol. 54*, 313−326.

27. Baker, J. E., LaConte, L. E. W., Brust-Mascher, I., and Thomas, D. D. (1999) *Biophys. J.* (in press).

28. Wray, J. S., Vibert, P. J., and Cohen, C. (1975) *Nature 257*, 561−564.

29. Vibert, P. (1992) *J. Mol. Biol. 223*, 661−671.

30. Crowther, R. A., R. Padron, and Craig, R. (1985) *J. Mol. Biol. 184*, 429−439.

31. Stewart, M., Kensler, R. W., and Levine, R. J. C. (1985) *J. Cell Biol. 101*, 402−411.

32. Stewart, M., and Kensler, R. W. (1986) *J. Mol. Biol. 192*, 831−851.

33. Levine, R. J. C., Chantler, P. D. Kensler, R. W., and Yount, R. G. (1989) *Biophys. J. 55*, 82a.

34. Bagshaw, C. R. (1987) *Nature 326*, 746−747.

35. Harada, Y., Noguchi, A., Kishino, A., and Yanagida, T. (1987) *Nature 326*, 805−808.

36. Ito, K., Liu, X., Katayama, E., and Uyeda, T. Q. P. (1999) *Biophys. J. 76*, 985−992.

37. Kalabokis, V. N., and Szent-Györgyi, A. G. (1997) *Biochemistry 36*, 15834−15840.

38. Conibear, P. B., and Geeves, M. A. (1998) *Biophys. J. 75*, 926−937.

39. Smith, C. A., and Rayment, I. (1995) *Biochemistry 34*, 8973−8981.

40. Smith, C. A., and Rayment, I. (1996) *Biochemistry 35*, 5404−5417.

41. Gulick, A. M., Bauer, C. B., Thoden, J. B., and Rayment, I. (1997) *Biochemistry 36*, 11619−11628.

42. Dominguez, R., Freyzon, Y., Trybus, K. M., and Cohen, C. (1998) *Cell 94*, 559−571.

43. Houdusse, A., Kalabokis, V. N., Himmel, D., Szent-Györgyi, A. G., and Cohen, C. (1999) *Cell 97*, 459−470.

44. Rayment, I., Rypniewski, W. R., Schmidt-Base, K., Smith, R., Tomchick, D. R., Benning, M. M., Winkelmann, D. A., Wesenberg, G., and Holden, H. M. (1993) *Science 261*, 50−58.

45. Holmes, K. C. (1998) in *The Limits of Reductionism in Biology. Novartis Foundation Symposium*, vol. 213, pp 76−92, Wiley, Chichester.

46. Wells, C., and Bagshaw, C. R. (1983) *J. Mol. Biol. 164*, 137−157.

47. Cooke, R., Crowder, M. S., and Thomas, D. D. (1982) *Nature 300*, 776−778.

48. Fajer, P. G., Fajer, E. A., Schoenberg, M., and Thomas, D. D. (1991) *Biophys. J. 60*, 642−649.

49. Barnett, V. A., and Thomas, D. D. (1989) *Biophys. J. 56*, 517−523.

50. Berger, C. L., and Thomas, D. D. (1994) *Biophys. J. 67*, 250−261.

51. Roopnarine, O., and Thomas, D. D. (1996) *Biophys. J. 70*, 2795−2806.

52. Roopnarine, O., Szent-Gyorgyi, A. G., and Thomas, D. D. (1998) *Biochemistry 37*, 14428−14436.

53. Ramachandran, S., and Thomas, D. D. (1999) *Biochemistry* (in press).

54. Vibert, P., and Cohen, C.(1988) *J. Muscle Res. Cell Motil. 9*, 296−305.

55. Adhikari, B., Hideg, K., and Fajer, P. (1997) *Proc. Natl. Acad. Sci. U.S.A. 94*, 9643−9647.

56. Whittaker, M., Wilson-Kubalek, E. M., Smith, J. E., Faust L., Milligan, R. A., and Sweeney, H. L. (1995) *Nature 378*, 748−751.

57. Burgess, S. A., Walker, M. L., White, H. D., and Trinick, J.- (1997) *J. Cell Biol. 139*, 675−681.

58. Holmes, K. C. (1996) *Curr. Biol. 7*, R112−R118.

59. Bennett, W. S., and Huber, R. (1984) *CRC Crit. Rev. Biochem. 15*, 291−384.